



DEFORMATION BEHAVIORS INVESTIGATION OF CoCr ALLOY LATTICE STRUCTURES UNDER COMPRESSION TEST

*Özgün Ceren Akbay¹, Burak Özdemir², Erkan Bahçe¹, Ender Emir³

¹Inönü University, Faculty of Engineering, Mechanical Engineering Department Malatya, Turkey

²Malatya Turgut Özal University Hekimhan MES Vocational School, Malatya, Turkey

³Kahramanmaraş Istiklal University, Elbistan Vocational School, Kahramanmaraş, Turkey

ABSTRACT

With the development of the additive manufacturing method, the production of lattice structures with complex geometries attracts increasing attention. These lattice structures can be designed with the desired properties, and they are encountered in many areas such as automotive, aerospace and aviation, and manufacturing industries, as they offer the freedom to control their physical, mechanical and geometric properties. The high strength characteristic of lattice structures that can be designed at any scale makes these structures useful for producing different designs. Since the mechanical responses of the lattice structures depend on the lattice design parameters, such as the large number of independent struts forming the lattice, cell size and cell geometry, the mechanical behaviour of these structures should be examined. In this study, a porous lattice structure with four different cell models, namely Dode Medium, Diamond, Rhombic Dodecahedron, and Dode Thin, was produced by Selective Laser Melting (SLM) method. In order to reveal the mechanical properties and deformation responses of the porous lattice structures, they were analyzed under compression test and by the finite element method, and experimental and numerical procedures were compared. The effect of the compression test on the lattice properties and how the deformation is distributed throughout the lattice structure were investigated. The finite Element Analysis and Digital Image Processing (DIP) method was used to determine how the lattices deform. The results obtained will be useful for designing new metallic lattice structures with more excellent deformation resistance in future studies.

Keywords: *Lattice Structures, Compression Test and Digital Image Processing*

1. Introduction

Advances in additive manufacturing have led to the ability to create new models with the freedom to control the design of lattice structures. Advanced design optimization is an important criterion in structures produced with additive manufacturing. Thanks to the control of the design parameters of the lattice structures, their mechanical, physical and thermal properties can vary [1]. These design parameters are depend on the internal architecture of the cellular structure, the cell model, size, and properties of the parent material used in production. For example, polymer structures with random cell arrangement often exhibit bending-dominant behavior in cell supports during elastic loading [2] or bending bending appears to be the dominant behavior in beams and struts during elastic loading in metal three-dimensional truss structures [3]. Therefore, although the main production material used

in additive manufacturing varies, it is important to analyze the mechanical performance of the parts. In particular, it is important to know more about how the behavior of metal lattice structures under mechanical tests is affected by design parameters. Considering the studies in the literature on this subject; Doyoyo et al. investigated the effects of ruptures caused by plastic yielding and elastic buckling on both tensile and bending responses in metallic lattices subjected to multiaxial loads [4]. Nayfeh et al. The octettruss and the mechanical analysis of the stresses occurring in the struts of a two-dimensional model. The analyzes showed that the elastic properties of both models are relatively close to each other [5]. Wang et al. They developed a mathematical method to show the relationship between the characteristic parameters of porous structures and their mechanical properties. They fabricated the porous structures with a 3D metal printer and tested their mechanical properties under varying

*Corresponding Author - E-mail: ceren.akbay@gmail.com

axial loads. According to the results of these tests, they concluded that a design with a porous structure increases the biomechanical performance, and its mechanical properties change as the pore diameter and density change [6]. Mehboob et al. The produced lattice structures were subjected to tests under compression, bending and torsional loads. They determined that the structures with a pore ratio of 47.3% showed the best mechanical properties [7]. Ghahramanzadeh et al. developed a model using finite element analysis to optimize the pore diameter of the porous structure and determined the optimum pore diameter as $35\mu\text{m}$ [8] Soro et al. The mechanical properties of titanium scaffolds with 60% and 70% porosity levels were investigated by finite element analysis under compressive loads. As a result of the analysis, they emphasized the importance that the stress distribution of porous scaffolds depends on the pore shape and pore diameter [9]. Akbay et al. performed compression tests on porous models with varying cell density and shape geometry using different unit cell models. As a result of the tests, it was investigated how the deformation was distributed along the scaffolds and the results of the changing cell models were compared [10]. In addition to experimental measurements, Wallach et al. worked on unit cell modeling to calculate the elastic modulus, uniaxial compressive strength and shear strength of sandwich structures with pyramidal lattice cores [11]. As can be seen in the literature, studies on the design parameters of porous lattice structures are quite common. In this study, the effect of cell geometry change on the lattice properties, the deformation response under compression test and how the deformation is distributed along the lattice were investigated. The deformation response and the resulting error patterns on the models displayed using a high-speed camera were examined. Finite element analysis method was used and simulations were made to understand the relationship of material strain rate with the change of unit cell models. The Digital Image Processing (DIP) method was used to obtain information about how the lattices were deformed. Figure 1 illustrates the methodology of the present work.

2. Methodology

2.1 Design of Lattice Structures

In this study, four different lattice structures, namely Diamond, Dode Medium, Dode Thin and Rhombic Dodecahedron, are discussed. The porous models designed using Computer Aided Design software were saved in STL format and transferred to a Concept Laser metal printer. The unit lattice cells, the

cellular cubes obtained for each unit lattice, isometric and front views for each lattice structure are shown in Figure 2 together with the lattice dimensions (mm). According to the design, the number of struts and the strut diameter of the porous models are given in Table.1.

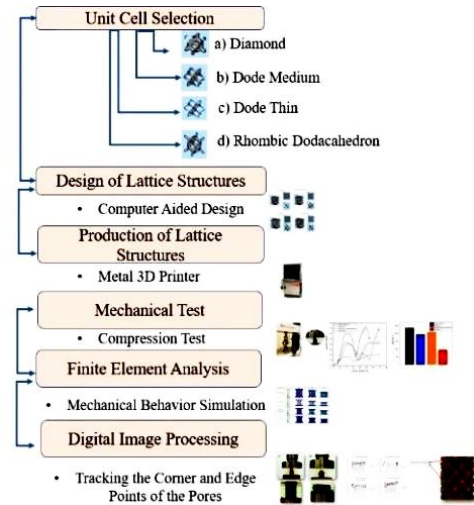


Fig. 1 Methodology

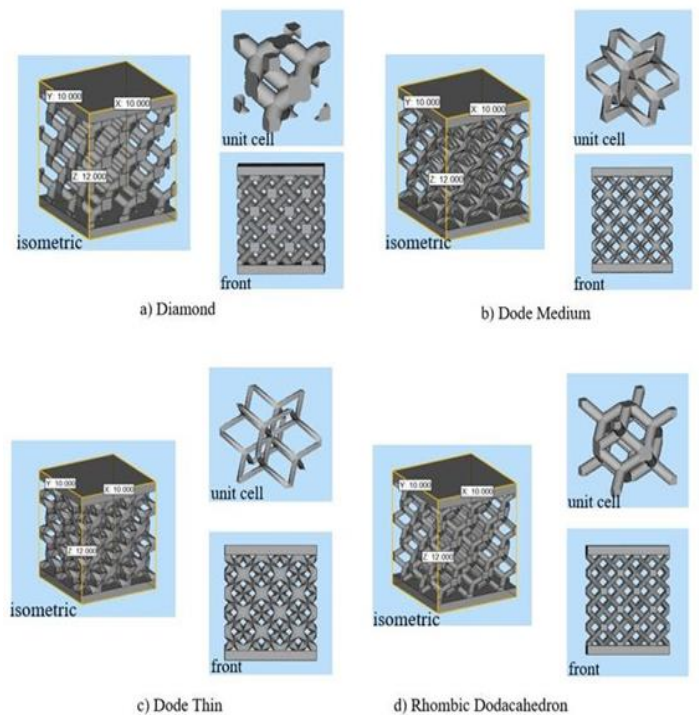


Fig. 2 Unit Cell Models and Lattice Designs of Porous Models a) Diamond b) Dode Medium c) Dode Thin d) Rhombic Dodacahedron

Table 1 Number of Struts and Diameters of Porous Models

Model Names	Number of Strut	Strut Diameter (mm)
Diamond	13531	4.73
Dode Medium	13948	4.53
Dode Thin	11388	4.16
Rhombic	8664	4.36
Dodacahedron		

High purity argon gas was used as the shielding gas to make the oxygen content in the environment less than 0.1% throughout the production process. SLM processing parameters are shown in Table.2. After fabrication the porous lattice structures were allowed to cool at room temperature and then fabricated models were cut from the substrate using a wire electric discharge machining (EDM) process.

Table 2 Machining Parameters

Property	Value
Layer Thickness (Minimum)	15 – 30 μm
Laser System	Fiber Laser
Focal Diameter	50 μm
Inert Gases	Argon
Maximum Scanning Speed	7 m/s

2.2 Compression Test

Compression tests were performed to investigate the deformation behaviour of each lattice structure. SHIMADZU AG-IC device was used to perform the compression tests. (Fig. 3) The compression speed is set to 10 mm/min and the ramp speed of the machine is set to 0.07 mm/min. Compression tests were carried out until the force decreased with increasing displacement. In order to minimize the friction force on the contact surfaces of the porous models, a flat plate is placed on the unit to be tested.

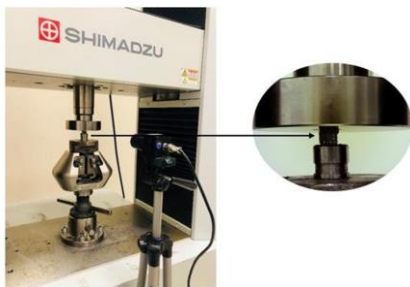


Fig. 3 SHIMADZU AG-IC Compression Test Machine and Test Sample Example

Porous models are placed in the middle of the plate to ensure that the displacement is applied evenly. The lattice deformation was characterized using an image processing method used to track the displacements of predefined points on the models. Images were recorded with an ELP brand 8 MP camera. The camera is positioned at a distance of 80 mm from the workpiece and fixed focus. During the compression test, load-displacement curves were analyzed to compare the deformation behaviour of the porous models via yield and condensation points. The condensation point of the porous structures was defined as the location where adjacent buttresses began to come into contact with each other so that the measured displacements were then used to calculate the axial and lateral deformation of the models. Data from the compression test were exported and analyzed in Microsoft Excel.

2.3 Finite Element Analysis

To ensure that the simulation conditions are consistent with the compression test, the finite element analysis method simulated the mechanical behavior under the compression test on full-size models of four different porous lattice structures. The force and boundary conditions to be applied to porous structures have been determined by considering the literature [12-14]. CoCr was chosen as the material. A tetrahedral mesh with an average size of 0.5 mm was used to model the four structures. End plates of minimum thickness were placed on the top and bottom of the model to ensure that the overall mechanical properties were not affected before the load was applied. The simulation process is as similar as possible to the actual test (Fig. 4). Simulation was performed at the same loading speed as the experiment. The model was fixed by applying full restraint to the bottom plate for uniform distribution of the load.

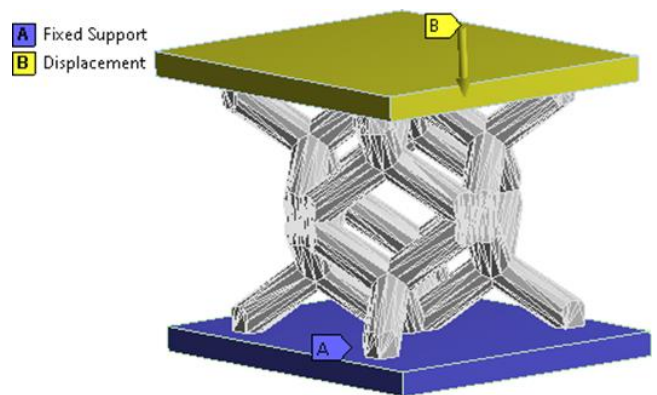


Fig. 4 Example of Finite Element Analysis

2.4 Digital Image Processing

To assess the reliability of digital image processing, a preflight was applied before each run was tested. The displacement of a point in the porous structures during the compression test takes different values depending on the position of the fixed and movable jaws, so the maximum displacement corresponds to the end portion of the porous models facing the movable jaw. The minimum displacement is positioned to correspond to the fixed jaw-facing portion. Point tracking was applied to the images taken with the camera within the image processing method. Before the compression test, a point was assigned to the corners and edges of the samples. (Fig.4a) The attributes of these points are recorded in the program, and the displacement amounts of the points are calculated as the image progresses. The new position of the tracked point is marked in each frame of the image. (Fig.4b) As a result of the experiment, the unit deformation was calculated by using the axial total displacement values of the points (Equation 1).

$$d = \sqrt{(x_1 - x_2)^2 + (y_1 - y_2)^2} \quad d_b = \frac{d}{n} \quad (1)$$

(x1,y1) and (x2,y2) given in the equation represent the first and last coordinate values of the points. The value of the displacement amount of the points in pixels is expressed by d. The number of points is n and db is the unit displacement amount.

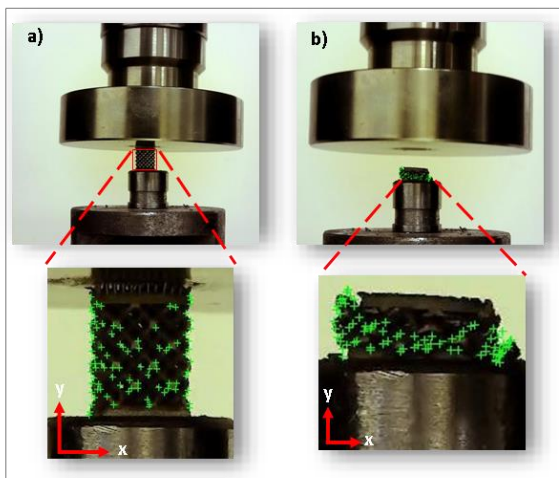


Fig. 5 Tracking the Corner and Edge Points of the Pores with the Digital Image Processing Method a) Before Compression Test b) After Compression Test

Figure 5 shows the displacement versus time measured by the DIC and reported by the machine for a control sample. Both curves are linear in time as a constant rate of displacement is applied. For both configurations, maximum deformation and maximum stress were observed at the crack tips. A maximum deviation of 3% was found between the two samples.

3. Discussion And Results

3.1. Compression Test Results

All compression tests were performed under a load of 100 kN, with a data rate of 10 points/s and a ramp rate of 0.07 inches/min of the machine to ensure full deformation. The produced porous lattice structures were placed between two fixed plates in the compression test device, and the compression test was repeated. The values obtained as a result of the compression test were calculated as shown in Equation 2 and Equation 3, and the Stress – Percent Elongation graph was created.

$$\sigma_b = P_i / A_0 \quad (2)$$

$$e_b = (l_i - l_0) / l_0 = \Delta l / l \quad (3)$$

Stress-Percent Elongation graph of porous models is given in Figure. 6. In the porous models; the stress was measured as 73.6 MPa in the highest Diamond model and 19.9 MPa in the lowest Dode Thin model. The Dode Medium model reached the maximum stress during the experiment, but the compression test could not be continued because the deformation response of the model resulted in sudden breakage.

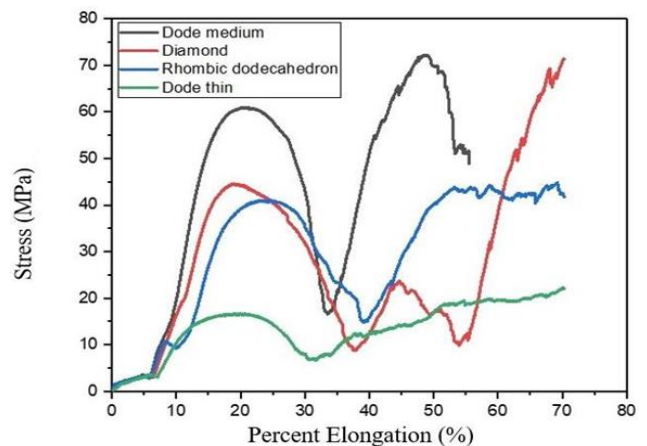


Fig. 6 Stress-Percent Elongation Graph of Porous Models

Three tests were performed on each sample to obtain statistically correct results and both mean and standard deviation values are given in Table.3. The stresses in the porous models peaked at low strains and decreased until the onset of a second peak value. It can be easily understood that these peak stress values are evidence of the existence of the stress-dominated collapse mechanism. Another finding that should be taken into account is that the stress peaks lose their visibility as the unit cell size decreases.

Table 3 Porosity Ratio, Average Compressive Strength and Maximum Compressive Strength Values of Porous Lattice Models

Model Names	Sample Porosity Ratio (%)	Average Compressive Strength (Mpa)	StandardDeviation Ratio (%)	Maximum Compressive Strength (Mpa)
Dode Medium	82.1	58.7	2.1	72.9
Diamond	85.8	64.3	1.7	73.6
Rhombic Dodecahedron	84.9	34.5	1.5	45.3
Dode Thin	80.5	12.4	2.2	19.9

When the stress – percent elongation curves of porous lattice structures are examined, it is seen that three different regions occur for all four lattice structures in the case of compressive loading. (Fig.7)

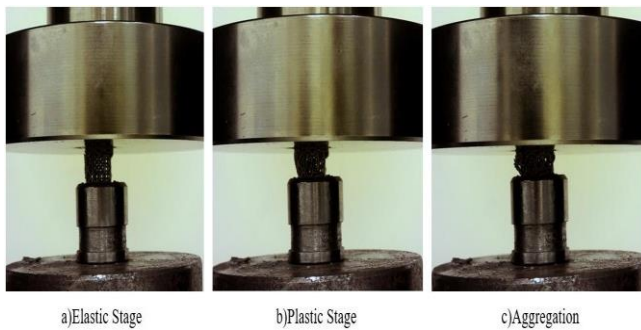


Fig. 7 Example of Three-Stage Deformation of Porous Lattice Structures a) Elastic Deformation Phase b) Plastic Deformation Phase c) Aggregation Phase

As a result of the compression tests, it is seen that the material changes at a certain rate in response to the increasing stress. The first deformation that occurs is elastic, and the unit deformation that occurs in response to the applied stress in this region changes linearly. Some struts in the porous structure showed a tendency to collapse at the end of the first zone (Fig. 6a). While the stress value in the plastic region remains approximately constant for a long time, the deformation continues. Plastic deformation occurs continuously until all cells collapse completely. The deformation that occurred at the end of the second region is not reversible, that is, the plastic deformation has occurred (Fig.7b). In this region, called the aggregation phase, the stress increased rapidly in a steep manner.

The toughness values were calculated to find the porous models' plastic deformation ability and the energy absorbed until the breaking point. According to the stress results shown in Figure 5, the fastest deforming model is the Dode Thin model, and the toughness value decreased as the deformation rate increased. Dode Thin model gave the lowest stress values and in parallel with this situation, the lowest toughness value was seen in the Dode Thin model. (Fig.8)

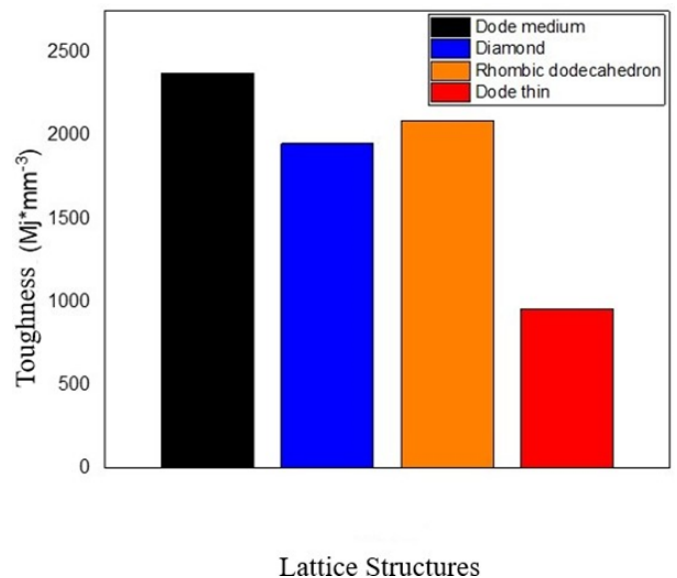


Fig. 8 Toughness Values of Porous Lattice Structures

The plastic deformation that occurs in porous models depends on the high energy absorption capability of the structure. High energy absorption ability at high-impact velocities is the main objective in such porous structures [15]. Therefore, compression tests are performed to verify the suitability of lattice structures as energy absorbers at high-impact velocities. Since the collapse point of the truss structures are the points where the stress is maximum, they are typically where the struts are connected to each other. Observation of cracked surfaces under the compression test indicates plastic deformation, although this is difficult to detect consistently and with high pressure, cracking was observed in the parts of the struts far from each other, which is supported by the literature [16].

3.2 Finite Element Analysis Results

The finite element analysis method was used to analyze the deformation occurring in four porous lattice structures under the same load. This study provided the theoretical basis for the impact strength capacities of porous lattice structures.

Three boundary conditions were assigned to the porous models before analysis. First, a flat surface is determined at the base of the porous model, which prevents any displacement in the direction of the applied force. The second boundary condition was fixed at the plate corresponding to the desired strain at the top of the porous model. Third, a fixed attachment point that prevents lateral movement of the porous model was determined. The porous models were meshed with the tetrahedral structure model representing the size of the meshing elements, and the analysis was started after all necessary steps were completed. As a result of the analysis, it has been observed that the highest stress values occur especially in the places where the struts in the porous models join at small angles and around the nodes. Considering the studies in the literature, a quantitative comparison was made by comparing the ratio of the average stress (σ_{AVG}) calculated as the average of the maximum stress (σ_{MAX}) obtained in the middle of the uprights [17-19]. Figure.9 shows the stress distribution for porous lattice structures under compression loading.

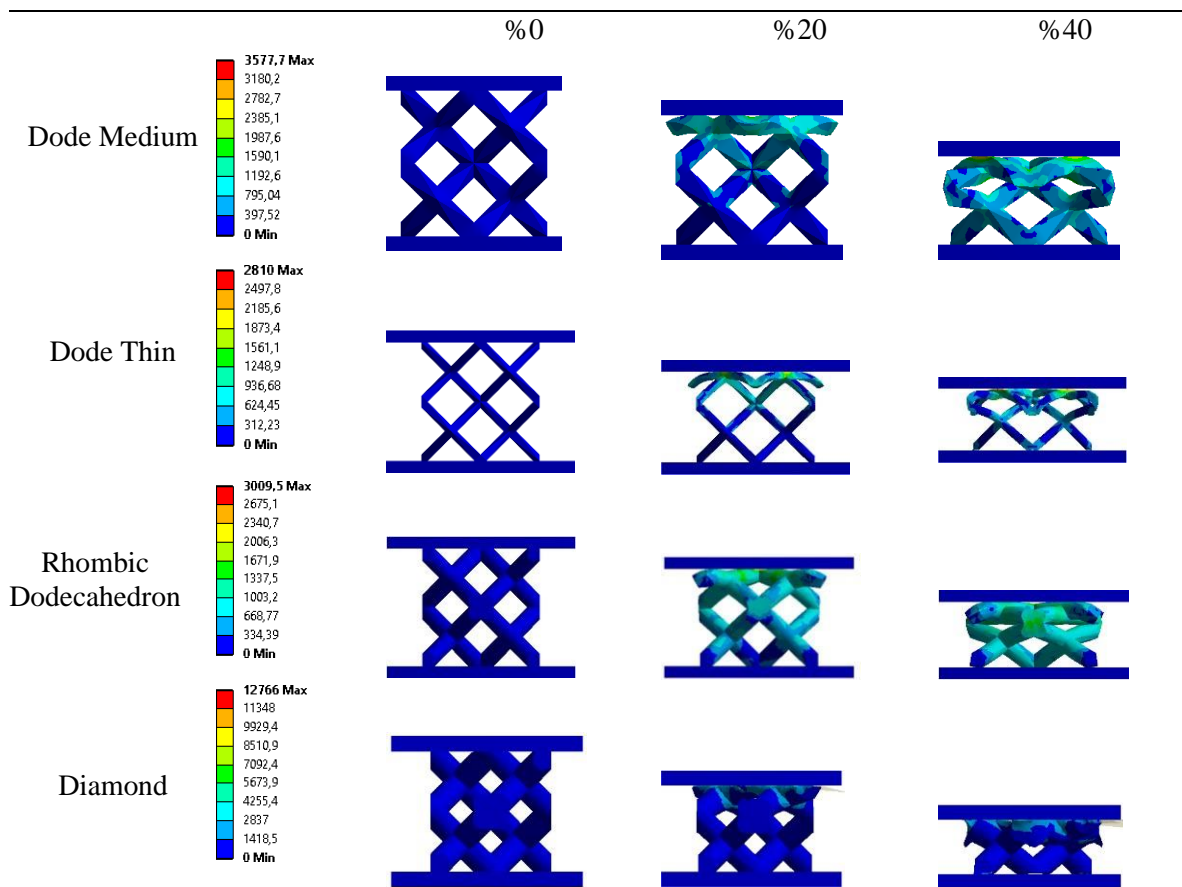


Fig. 9 Finite Element Analysis of Porous Models Compression Test Simulation Images

For the Diamond cell geometry, the stress values found (>12000 MPa) are roughly 4 times higher than the stress values found for the Dode Thin cell geometry. Similar stress levels were observed in Dode Medium and Rhombic Dodecahedron cell geometries. In addition, the ratio of maximum stress to average stress is around 1.60 for Dode Thin cell geometry and 1.14 for Diamond cell geometry (Table.3). This showed that there was a more even distribution of stress in the Diamond model, which was also supported by the literature [20]. Negative maximum principal stress (red color) was not observed on the vertical supports for all four lattice structures, indicating that all the struts of the lattice structures were compressed equally. [21,22]

3.3 Digital Image Processing Results

In the images taken during the compression test, the location of the endpoints along the x-axis and y-axis passing through the center of each pore of the samples are marked (Fig.10). By following these points, unit displacement amounts were calculated according to equation 1 at the end of the experiment (Table.4).

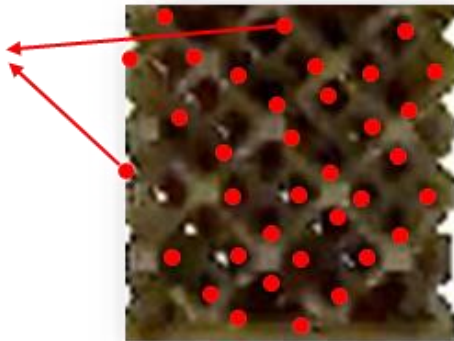


Fig. 10 Pore Deformation Tracking Points

Table 4 Unit Displacement Values of Tracked Points on the Samples

Model Names	Unit Displacement (d_b)
Diamond	32,643
Dode Medium	47,002
Dode Thin	58,347
Rhombic Dodecahedron	49,337

Pore damage is most visible in the Dode Thin sample. The lowest tensile strength of the Dode Thin specimen in the compression test and left element analysis confirms this result. The unit damage in the sample pores is as large as 45% of the image size. Similarly, the Diamond sample is the sample with the least pore damage in parallel with the compression test and finite element analysis. The pressure-resistant nature of the cell geometry ensured that the pore damage remained at the rate of approximately 25%. Dode Medium and Rhombic Dodecahedron samples had similar pore damage values (~36-38%). Sudden fracture effect is observed in both samples. Damages started with crack initiation at the nodes highlighted in red in Figure 10. Similar deformation responses were observed in all porous specimens subjected to the compression test. Local shear deformation was observed in the structure in the porous models with compressive stress (Fig.11).

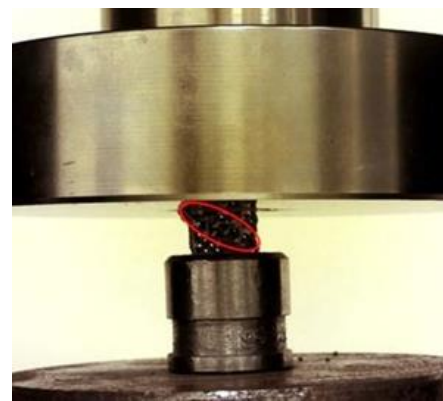


Fig. 11 Local Shear Deformation Example

Although compression deformation areas were observed in different parts of the models, collapses occurred at the node locations. In the porous structures, fracture occurred at approximately 45° according to the strain distributions. This shows that the models do not directly break under the compression test but instead break in the transitions between the struts. In the compression tests, it was observed that the stress increased with the increase in the number of unit cells and the strut diameters, and cracks formed when 45o inclination occurred after buckling [23]. The locations of the physical defects found were classified as point defects. (Fig.12)

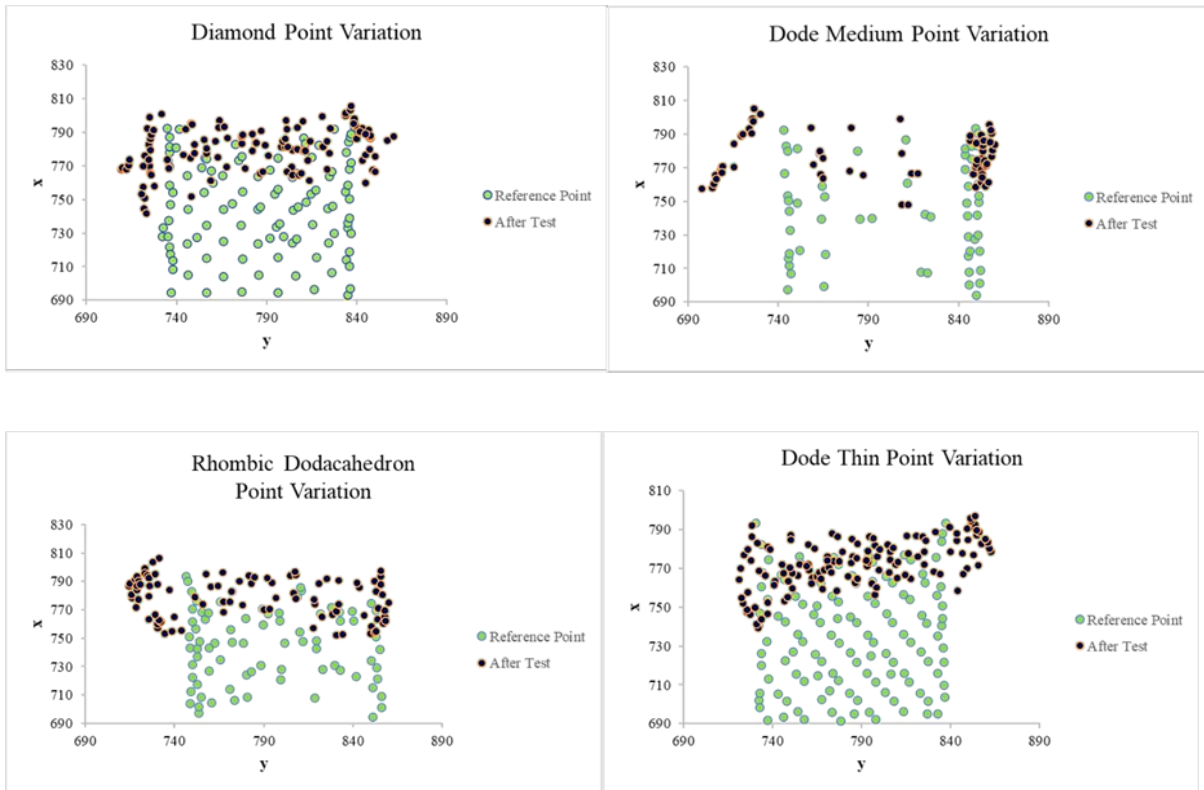


Fig. 12 Under Compression Test Pore Deformation Graphics

When point deformation is followed when the unit cell size increases, the number of cells in the porous lattice structure decreases. However, when the struts in the lattice structure are long, it has been observed that the part undergoes deformation during mechanical tests because the amount of protrusions in the structure is high [24]. Porous structures with a cross-lattice structure, such as Dode Thin, have been observed to have approximately 30% less strength than horizontal and vertical lattice structures, such as Diamond [25]. The analysis of the distribution of stresses around the nodes of the lattice structures more clearly understands the behaviour of the porous lattice structures during the compression test. Stress distributions occurring in various parts of porous structures are shown with point densities in the same part. The point deformation analysis allowed us to examine the behaviour of the unit cell geometries constituting the porous lattice structures under the compression test. It gave information about the density distribution of the plastic deformation passing through the nodal centres of the lattice structures (Figure 12).

Plastic deformation has been observed intensively in the nodes of the unit cells and the studies in the literature have supported that the deformation of the lattice structures during compression is due to the rotation of the axes in the nodes [26].

4. Results

The SLM method produced the lattice structure with four different unit cell models made of CoCr alloy, and its deformation behaviours were investigated under compression tests and simulations. The stress-percent elongation curve for porous lattice structures was determined by the analysis of compression tests. Based on the results of the compression tests of the porous lattice structures, the deformation occurred in three stages. The stress distribution at the nodes of the lattice structures first caused elastic deformation depending on the unit cell model used. As the compression test continued, the cells decreased in size, and the second stage, plastic deformation, was observed with compression. Then, the aggregation phase was observed as the unit cells were stacked on each other. The

simulation results obtained from the finite element analysis agreed with the experimental results; thus, it has been a guide to determine the desired mechanical properties of the porous lattice structures in future studies. A sensitive camera was used during the compression test, and it was observed that all lattice structures did not form obvious macro defects, such as large cracks. Since the lattice structures deform and break along the force direction when the load is applied, the angle and unit cell model at which the struts are connected in each unit cell should be determined by considering the deformation response of the struts after the load is applied to the porous lattice structures. The dependence of the mechanical properties on the lattice design parameters used has been a reference for future studies. In future research, more unit cell models with varying densities and load states will be explored using different materials to analyze porous lattice structures.

References

1. Maconachie, T., Leary, M., Lozanovski, B., Zhang, X., Qian, M., Faruque, O., & Brandt, M. (2019). SLM lattice structures: Properties, performance, applications and challenges. *Materials & Design*, 183, 108137.
2. Gümrük, R., Maden, RAW ve Karadeniz, S. (2013). Paslanmaz çelik mikro kafes yapıların farklı yüklemeye koşulları altında statik mekanik davranışları. *Malzeme Bilimi ve Mühendisliği: A*, 586, 392-406.
3. Jacobsen, A. J., Barvosa-Carter, W., & Nutt, S. (2008). Micro-scale truss structures with three-fold and six-fold symmetry formed from self-propagating polymer waveguides. *Acta Materialia*, 56(11), 2540-2548.
4. Doyoyo, M. ve Hu, JW (2006). Kısa ve ince dikmelerden oluşan metalik dikme-kafes malzemelerinin çok eksenli arızası. *Uluslararası katılar ve yapılar dergisi*, 43 (20), 6115- 6139.
5. Nayfeh, AH ve Hefzy, MS (1978). Üç boyutlu kafes benzeri uzay yapılarının sürekli modellenmesi. *Aiaa dergisi*, 16 (8), 779-787.
6. Wang, C., Huang, W., Zhou, Y., He, L., He, Z., Chen, Z., ... & Wang, M. (2020). 3D printing of bone tissue engineering scaffolds. *Bioactive materials*, 5(1), 82-91.
7. Mehboob, H., Tarlochan, F., Mehboob, A., & Chang, SH (2018). Çimentosuz biyomimetik gözenekli kalça sapının tasarımı için 3B hücresel mikro yapıların sonlu eleman modellemesi ve karakterizasyonu. *Malzemeler ve Tasarım*, 149, 101-112.
8. ASL, H. G., YILMAZ, S., & Ertuğrul, SARI. Gözenekli Yapıya Sahip Kalça Protezi Tasarımı ve Uyluk Kemiği Üzerinde Sonlu Elemanlar Analizi. *Erzincan University Journal of Science and Technology*, 12(1), 95-105.
9. Soro, N., Brassart, L., Chen, Y., Veidt, M., Attar, H., & Dargusch, M. S. (2018). Finite element analysis of porous commercially pure titanium for biomedical implant application. *Materials Science and Engineering: A*, 725, 43-50.
10. Akbay, Ö. C., Bahce, E., & Ölmez, C. (2022). Investigation of Mechanical Behavior of Scaffolding Structures Produced Using CoCr Alloy by Selective Laser Melting Method. *ICONTECH INTERNATIONAL JOURNAL*, 6(2), 18-26.
11. J.C. Wallach, L.G. Gibson, *Mechanical behavior of a three-dimensional truss material*, *Int.J. SolidsStrut.*38(2001) 7181-7196.
12. Wang, L., Kang, J., Sun, C., Li, D., Cao, Y., & Jin, Z. (2017). Mapping porous microstructures to yield desired mechanical properties for application in 3D printed bone scaffolds and orthopaedic implants. *Materials & Design*, 133, 62-68.
13. Dumas, M., Terriault, P., & Brailovski, V. (2017). Modelling and characterization of a porosity graded lattice structure for additively manufactured biomaterials. *Materials & Design*, 121, 383-392.
14. Quevedo González, F. J., & Nuño, N. (2016). Finite element modelling approaches for well-ordered porous metallic materials for orthopaedic applications: cost effectiveness and geometrical considerations. *Computer methods in Biomechanics and Biomedical engineering*, 19(8), 845-854.
15. Merkt, S., Hinke, C., Bültmann, J., Brandt, M., & Xie, YM (2015). Selektif lazer ergitime ile üretilen TiAl6V4 kafes yapılarının yarı statik ve dinamik basma testlerinde mekanik tepkisi. *Lazer uygulamaları günlüğü*, 27 (S1), S17006.
16. Goodall, R., Hernandez-Nava, E., Jenkins, SN, Sinclair, L., Tyrwhitt-Jones, E., Khodadadi, MA, ... & Ghadbeigi, H. (2019). Ti6Al4V kafeslerin mekanik davranışındaki kusur ve hasarın etkileri. *Malzemelerdeki Sınırlar*, 6, 117.
17. Luxner, M. H., Stampfl, J., & Pettermann, H. E. (2007). Numerical simulations of 3D open cell structures—influence of structural irregularities on elasto-plasticity and deformation localization. *International Journal of Solids and Structures*, 44(9), 2990- 3003.
18. Karamooz Ravari, M. R., & Kadkhodaei, M. (2015). A computationally efficient modeling approach for predicting mechanical behavior of cellular lattice structures. *Journal of Materials Engineering and Performance*, 24(1), 245-252.
19. Ni, Z., Wang, Z., Sun, L., Li, B., & Zhao, Y. (2014). Synthesis of poly acrylic acid modified silver nanoparticles and their antimicrobial activities. *Materials Science and Engineering: C*, 41, 249-254.
20. Smith, M., Guan, Z., & Cantwell, W. J. (2013). Finite element modelling of the compressive response of lattice structures manufactured using the selective laser melting technique. *International Journal of Mechanical Sciences*, 67, 28-41.

21. Guo, X. E., & Gibson, L. J. (1999). Behavior of intact and damaged honeycombs: a finite element study. *International Journal of Mechanical Sciences*, 41(1), 85-105.
22. Luxner, M. H., Stampfl, J., & Pettermann, H. E. (2005). Finite element modeling concepts and linear analyses of 3D regular open cell structures. *Journal of Materials science*, 40(22), 5859-5866.
23. Yu, T., Hyer, H., Sohn, Y., Bai, Y., & Wu, D. (2019). Structure-property relationship in high strength and lightweight AlSi10Mg microlattices fabricated by selective laser melting. *Materials & Design*, 182, 108062.
24. Hao, L., Raymond, D., Yan, C., Hussein, A., & Young, P. (2011, September). Design and additive manufacturing of cellular lattice structures. In *The International Conference on Advanced Research in Virtual and Rapid Prototyping (VRAP)*. Taylor & Francis Group, Leiria (pp. 249-254).
25. Weißmann, V., Bader, R., Hansmann, H., & Laufer, N. (2016). Influence of the structural orientation on the mechanical properties of selective laser melted Ti6Al4V open-porous scaffolds. *Materials & Design*, 95, 188-197.
26. Isaenkova, M. G., Yudin, A. V., Rubanov, A. E., Osintsev, A. V., & Degadnikova, L. A. (2020). Deformation behavior modelling of lattice structures manufactured by a selective laser melting of 316L steel powder. *Journal of Materials Research and Technology*, 9(6), 15177-15184.